Supplementary Information for:

Exploring Cr and Molten Salt Interfacial Interaction for Molten Salt Applications

Xiaoyang Liu[1], Yang Liu[1], Luke D. Gibson[2], Mingyuan Ge[3], Daniel Olds[3], Denis Leshchev[3],

Jianming Bai[3], Anna Plonka[4], Phillip Halstenberg[5,6], Hui Zhong[3], Sanjit Ghose[3], Cheng-Hung Lin[1], Xiaoyin Zheng[1],

Xianghui Xiao[3], Wah-Keat Lee[3], Sheng Dai[5,6], German D. Samolyuk[7],

Vyacheslav S. Bryantsev[5,*], Anatoly I. Frenkel[1,4,*], Yu-chen Karen Chen-Wiegart[1,3,*]

1 Materials Science and Chemical Engineering, Stony Brook University, Stony Brook, NY
2 Computational Sciences and Engineering Division, Oak Ridge National Laboratory, Oak Ridge, TN
3 National Synchrotron Light Source II (NSLS-II), Brookhaven National Laboratory, Upton, NY
4 Chemistry Division, Brookhaven National Laboratory, Upton, NY
5 Chemical Sciences Division, Oak Ridge National Laboratory, Oak Ridge, TN
6 Department of Chemistry, University of Tennessee, Knoxville, TN
7 Materials Science and Technology Division, Oak Ridge National Laboratory, Oak Ridge, TN

*Corresponding authors:
Karen.Chen-Wiegart@stonybrook.edu, anatoly.frenkel@stonybrook.edu, bryantsevv@ornl.gov

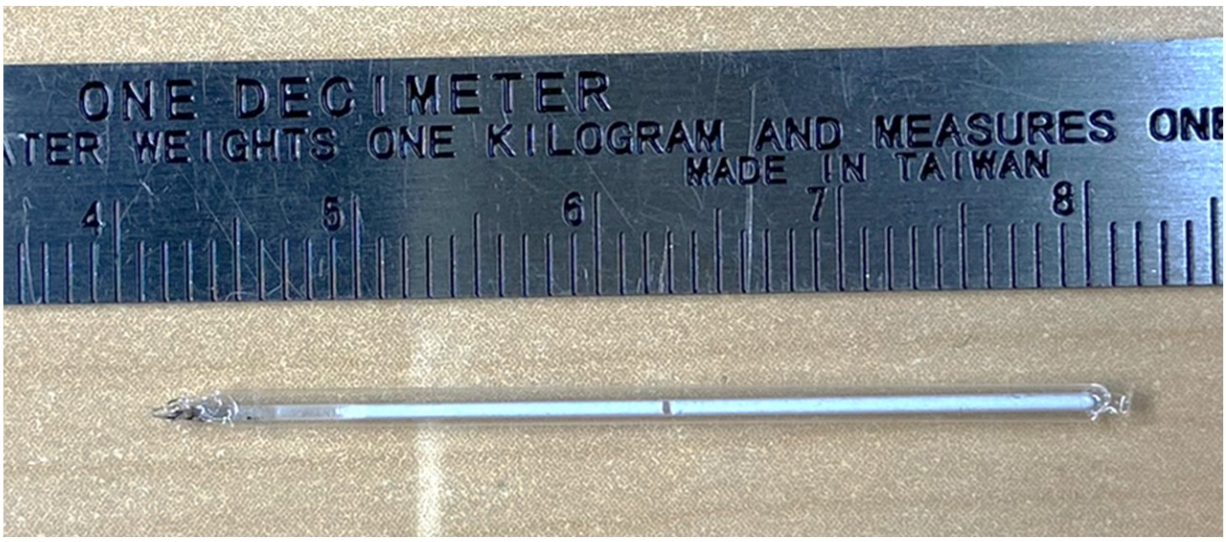

Figure S 1 – A photo of the sample (Cr powder in KCl-$MgCl_2$) for the X-ray diffraction experiment.

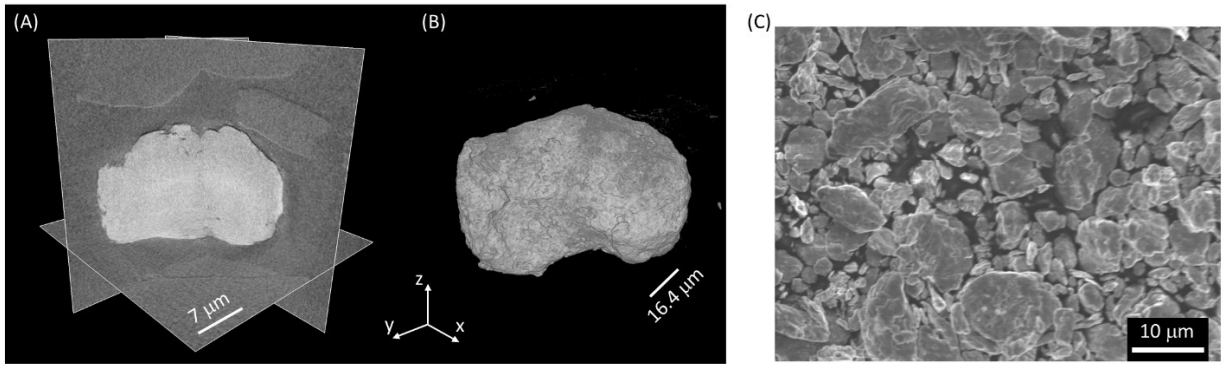

Figure S 2 – X-ray nano-tomography image of the pristine micro-sized Cr particle: (A) pseudo 2D cross-sectional view, and 3D volume rendering view. The pristine particle is irregular in shape with a small amount of internal cracks or voids, but it is still a solid particle, suggesting that most of the pores after molten salt corrosion are from the dissolution of Cr. (C) The surface morphology of the Cr particles imaged by SEM.

Density functional theory (DFT), ab initio molecular dynamics (AIMD), and phonon calculations

All density functional theory (DFT) calculations were performed using Vienna Ab Initio Simulation Package (VASP) version 6.2.1.[1-4] The gradient-corrected functional of Perdew-Burke-Ernzerhof (PBE)[5, 6] was employed, which has previously been shown to accurately describe the ground state properties of chromium.[7-11] While the PBE functional generally underestimates band gaps due to self-interaction error[12], the system studied herein—Cr metal (no band gap) and molten $MgCl_2$-KCl (very high band gap)—is largely unaffected by this deficiency. However, the effects of self-interaction error would need to be addressed for systems containing narrow band gaps (e.g., transition metal ions dissolved in molten salt) using methods such as DFT+U[13, 14] or Perdew-Zunger self-interaction correction[12, 15]. Valence electrons were expanded with plane waves and core-valence interactions were approximated with the projector augmented wave (PAW) method.[16, 17] In all cases, a plane wave kinetic energy cutoff value of 360 eV was used. Geometry optimizations were considered converged when the energy difference between two consecutive ionic steps was less than 10^{-4} eV. Electronic energy was considered converged when the energy difference between two consecutive self-consistent field (SCF) cycles was less than 10^{-5} eV. During phonon calculations, the SCF convergence criterion was increased to 10^{-8} eV instead. The Pulay mixing scheme[18] was used for charge density mixing during SCF calculations. During unit cell optimizations, the lattice length was the only degree of freedom due to symmetry. For slab optimizations, a vacuum gap of at least 20 Å was used to prevent self-interaction while all atomic positions were relaxed with fixed lattice parameters. The *k*-point mesh used in each calculation is described in their corresponding sections. Antiferromagnetism (AFM) was considered by enabling spin polarization and initializing the ordering of the magnetic moments in the appropriate alternating pattern. Paramagnetic systems were approximated by disabling spin polarization, which is referred to in the main text as "nonmagnetic." The justification for this approximation is provided in the section below.

Surface energies were computed using the following,

$$E_{surf} = \frac{E_{slab} - N\,E_{bulk}}{2A}, \#(1)$$

where E_{slab} is the total energy of the optimized slab, N is the number of chromium atoms in the slab, E_{bulk} is the energy per chromium atom in either bcc or δ-Cr phases, and A is the surface area of the slab system.

Adsorption energies for a KCl ion pair on relevant surfaces were computed herein using the following,

$$E_{ads} = E_{slab}^{KCl} - E_{slab}^{Vac} - E_{KCl}^{Vac}, \#(2)$$

where E_{slab}^{KCl} is the energy of the slab with KCl adsorbed onto the surface, E_{slab}^{Vac} is the energy of the optimized surface in vacuum, and E_{KCl}^{Vac} is the energy of a KCl contact ion pair in vacuum. The energy of a geometry-optimized KCl ion pair was computed with the same box size of the corresponding slab to eliminate the spurious contribution resulting from the interaction between the neighboring periodic images. The potassium pseudopotential included semi-core 3*s* and 3*p* states as valence states. Multiple placements of ions were tested for each surface and the most stable configurations are reported herein. K and Cl ions were confirmed to have negligible spin densities for spin-polarized calculations.

The average coordination numbers of Mg^{2+} and Cl^{-} with Cr surface atoms were computed with

$$CN(X,Cr) = \frac{1}{N_X}\sum_{i,j}\frac{1-\left(\frac{r_{X_i,Cr_j}}{r_0}\right)^{12}}{1-\left(\frac{r_{X_i,Cr_j}}{r_0}\right)^{24}}, \#(3)$$

where X_i represents the *i*th Mg^{2+} or Cl^{-} interfacial ion, r_{X_i,Cr_j} is the interatomic distance between the *i*th *X* ion and the *j*th Cr atom, N_X is the total number of interfacial *X* ions, and r_0 is the reference interatomic distance that determines the radius of included atoms (herein, we set $r_0 = 3$ Å).

Approximating Paramagnetic States as Nonmagnetic

Experiments were executed at 700 °C, well above the Néel temperature (37 °C) where bcc Cr becomes paramagnetic. One of the most accurate approximations of the paramagnetic state is the so called Disordered Local Moment (DLM) approximation.[19] In this approximation the paramagnetic state is modeled as a binary alloy with one component's magnetic moment ordering in the opposite direction. Applying the DLM approximation to bcc Cr, the two atoms in the unit cell are labeled as Cr(0,0,0) and Cr(0.5,0.5,0.5) and the two components have the following magnetic ordering:

Component A: +0.5 mB Cr(0,0,0) and -0.5 mB Cr(0.5,0.5,0.5)

Component B: -0.5 mB Cr(0,0,0) and +0.5 mB Cr(0.5,0.5,0.5)

The electronic structure of the $A_{0.5}B_{0.5}$ alloy can be solved using the coherent potential approximation (CPA).[20-22] As was demonstrated previously,[19] the self-consistent solution for Cr converges to a nonmagnetic state, in a contrast to Fe or Co, which is typical for weak magnets. Recently, Belozerov, *et al.* confirmed this finding using calculations that deployed a completely different approach.[11] Using state-of-the-art dynamical mean-field theory (DMFT) calculations, they were able to confirm that chromium is indeed a weak magnet with no formed local moments.

Taking into consideration the above discussion, we conclude that non-magnetic Cr is an adequate description of the bcc phase at 700 °C. The δ-A15 phase, however, has been found to be paramagnetic at all temperatures.[23] This could be explained by fact that the δ-A15 phase does not fulfill the Stoner criterion[24], which must be satisfied to form magnetic moments in itinerant magnets. According to the Stoner criterion, the product of the density of states at the Fermi energy (N) calculated in the nonmagnetic state and the exchange integral (I) should be greater than one. However, for the δ-A15 phase, $N = 0.8$ St/eV/atom and $I = 0.7$ eV.[25] As expected, attempts to converge the δ-A15 phase to either ferromagnetic or antiferromagnetic states resulted in a nonmagnetic state. Thus, all calculations of the δ-A15 phase were performed without spin polarization.

Bulk Optimizations

The bcc and δ-A15 Cr conventional cells were computed to have cubic cells with a lattice parameter of 2.86 and 4.54 Å, respectively, and their corresponding symmetry space groups are $Im\bar{3}m$ and $Pm\bar{3}n$. The Brillouin zone was sampled using a Γ-centered k-point mesh of 16×16×16 and 12×12×12 for bcc and δ-Cr, respectively.

Surface Energy Prediction

Slab models of each surface were generated from optimized unit cells and cleaved along appropriate directions using MedeA program.[26]

Equilibrating Systems in AIMD Simulations

AIMD simulations of KCl and $MgCl_2$ on (110)-bcc and (200)-δ-A15 surfaces were performed for ~12 ps each. The time series of potential energies for both systems are shown in Figure S3a,b. Block averaging[27] was used to assess the convergence of system energy, whereby the potential energies of all frames in a simulation are split into N consecutive blocks of size M and the mean values are computed for all blocks. The standard error of the mean can be computed from these mean values of potential energies. For correlated data (e.g., AIMD timeseries), the standard error of the mean will rapidly increase and then plateau as the block size (M) increases, which provides an estimate of the decorrelation time. Using the last 5 ps, the standard errors (of the mean potential energy) for increasing block sizes were computed and are shown in Figure S3c. The standard errors seem to plateau for block sizes of ~500+ frames, suggesting that the 5 ps window is stable. The (200)-δ-A15 system exhibits similar behavior when using an additional 2 ps (i.e., the last 7 ps), suggesting that the (200)-δ-A15 system reached an equilibrated state after ~5 ps. Although the (110)-bcc system needed ~7 ps to equilibrate the system's potential energy, analysis in the main text

was performed on the last 7 ps for both systems. The conclusions presented in the main text were confirmed to be consistent with analysis that was performed on only the last 5 ps.

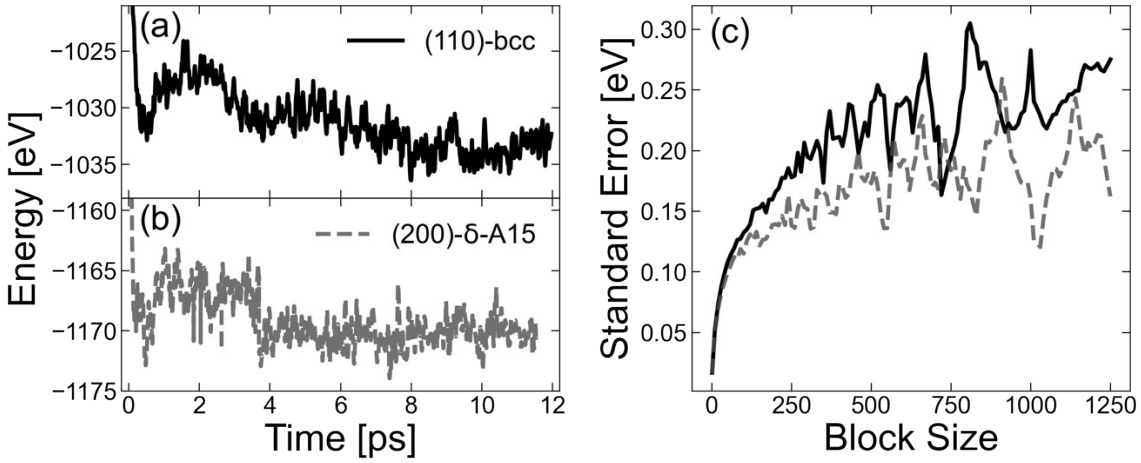

Figure S 3 – Potential energy during AIMD simulations of the KCl-$MgCl_2$ mixture on (a) (110)-bcc and (b) (200)-δ-A15 surfaces. (c) Standard errors from block averaging, where block size refers to the number of frames in each block.

Phase Thermodynamics

Phonon calculations were performed for bcc and δ-A15 Cr bulk systems to estimate temperature-dependent thermodynamic quantities such as the vibrational entropy and free energy using phonopy code.[28]

Potassium Chloride (KCl) Adsorption

To provide the initial understanding of how molten potassium chloride (KCl) can influence the stability of the chromium phases, we have computed KCl adsorption energies for (100)-bcc, (110)-bcc, and (200)-δ-A15 using Equation (2). The subsets of facets were chosen for each phase due to their greater stability over other facets and thus were more likely to be present in physical systems. In each case, multiple adsorption structures were tested and the most favorable structures for each surface are shown in this work. For both (100)-bcc and (200)-A15, larger supercells were used to more closely match the dimensions of the (110)-bcc surface. Instead of 3×3 and 2×2 supercells of (100)-bcc and (200)-δ-A15 in Figure 5A for surface energy calculations, larger 3×5 and 2×4 supercells were adopted for (100)-bcc and (200)-δ-A15,

respectively. This was necessary to avoid direct interaction between the ions in adjacent unit cells and attain lower absorption energies. The self-interaction of the KCl ion pair with neighboring images was further mitigated by using the corresponding box size for each slab system to compute the energy of an optimized KCl ion pair (i.e., KCl in the absence of the Cr slab). In doing so, we can establish qualitative trends in adsorption energy. The k-point meshes used for each slab system are listed in Table 1, while isolated KCl optimizations were performed with a 1×1×1 *k*-point mesh. Following adsorption optimizations, dipole corrections were computed and applied along the surface-normal direction for the optimized KCl-slab systems.

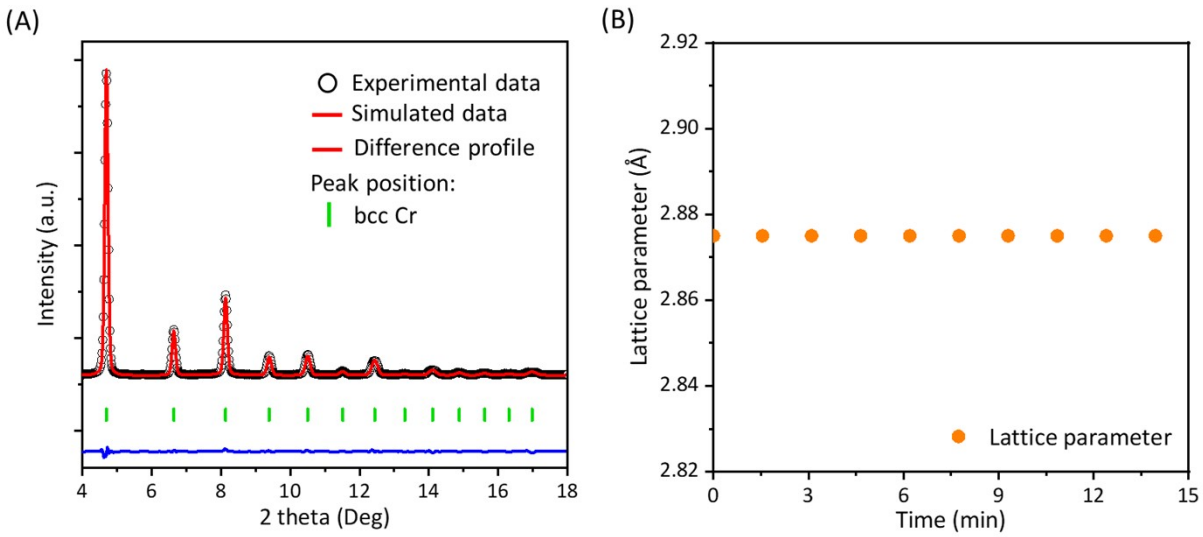

Figure S 4 - The diffraction pattern with Rietveld refinement of bcc Cr at 700 °C. (A) A representative of diffraction pattern collected for reaction at 14.0 min with Rietveld refinement. (B) The lattice parameter evolution of bcc Cr at 700 °C in Ar environment for ~14 min. The lattice parameter was 2.875 Å and did not change.

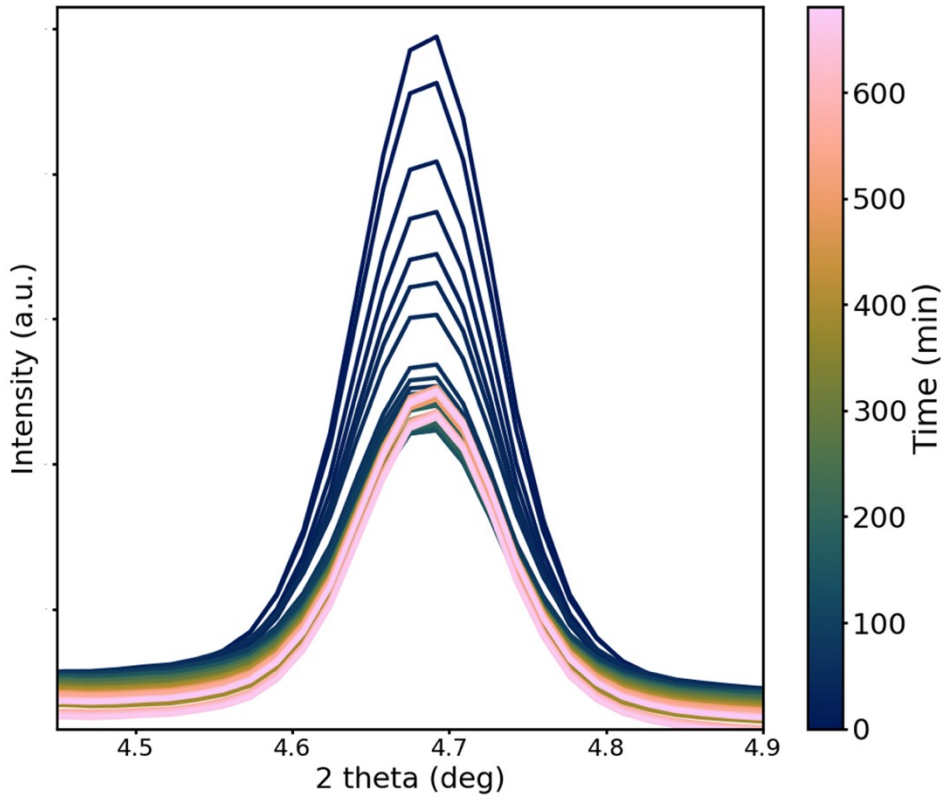

Figure S 5 – The diffraction intensity of bcc Cr (110) at 4.7 deg, the strongest peak, decreased in molten KCl-$MgCl_2$ (50-50 mol.%) at 700 °C, which indicates that the bcc Cr reacted in the molten salt.

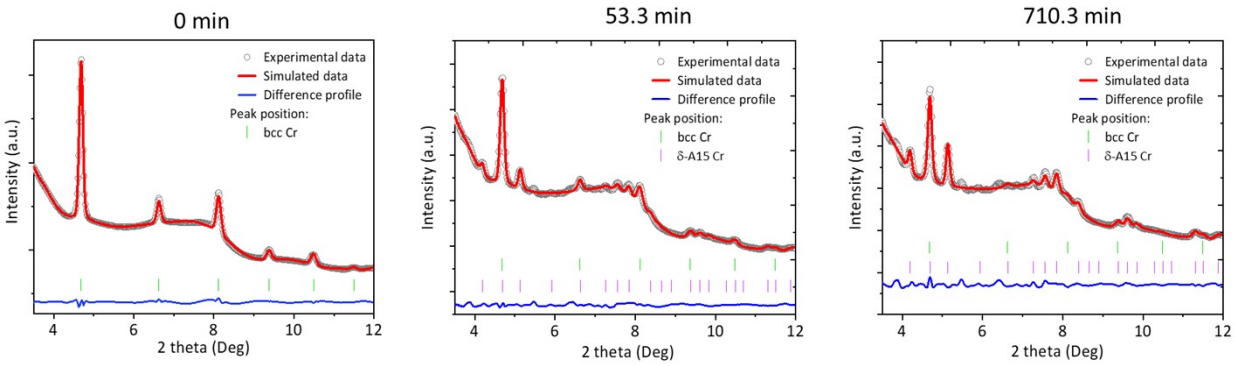

Figure S 6 – The Rietveld refinement for the dataset collected at 0, 53.3 and 710.3 min. At 0 min, bcc Cr was used for fitting. During the reaction, both bcc and δ-A15 Cr crystal structures were used.

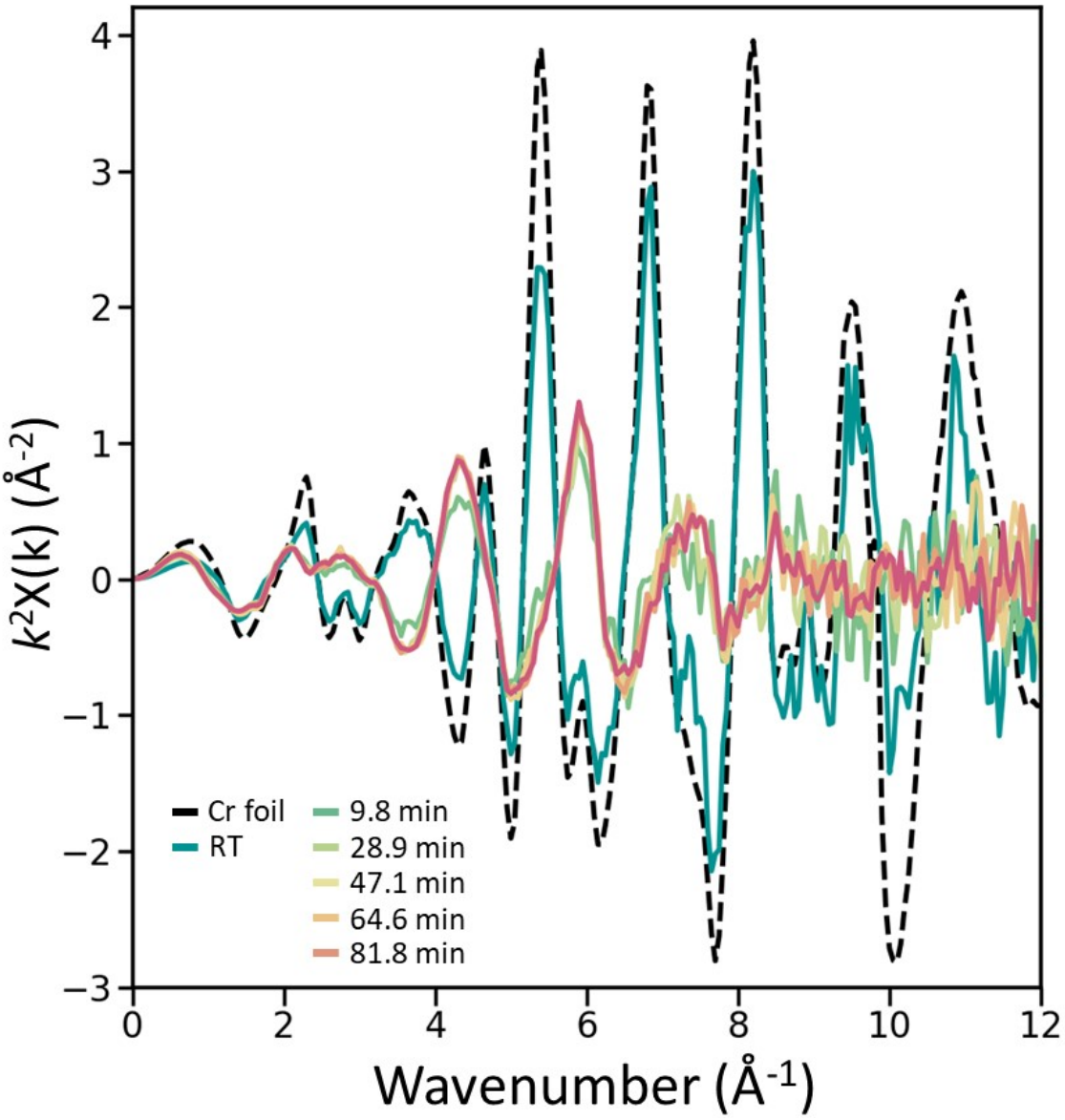

Figure S 7 – The Fourier transform of the *in situ* EXAFS to *k*-space.

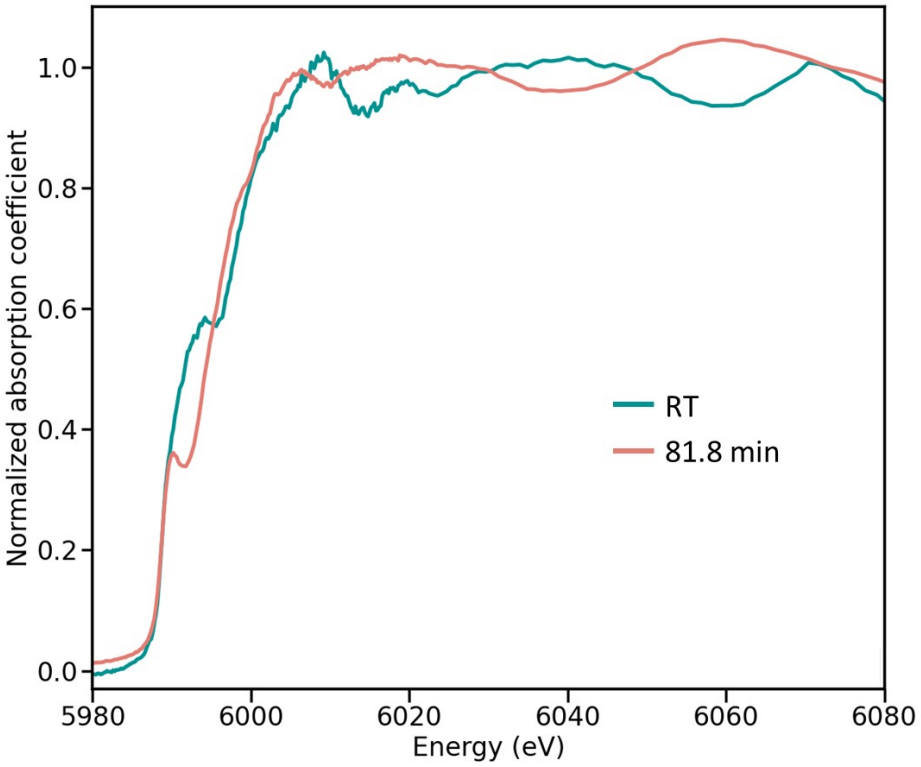

Figure S 8 – XANES spectra of bcc Cr at room temperature and reacted at 81.8 min emphasizes the difference of Cr structure after reaction in molten salt, which is consistent with the X-ray diffraction results.

References

1. G. Kresse and J. Furthmuller, Efficiency of ab-initio total energy calculations for metals and semiconductors using a plane-wave basis set, *Computational Materials Science*, 1996, **6**, 15-50.
2. G. Kresse and J. Furthmuller, Efficient iterative schemes for ab initio total-energy calculations using a plane-wave basis set, *Physical Review B*, 1996, **54**, 11169-11186.
3. G. Kresse and J. Hafner, AB-INITIO MOLECULAR-DYNAMICS SIMULATION OF THE LIQUID-METAL AMORPHOUS-SEMICONDUCTOR TRANSITION IN GERMANIUM, *Physical Review B*, 1994, **49**, 14251-14269.
4. G. Kresse and J. Hafner, AB-INITIO MOLECULAR-DYNAMICS FOR OPEN-SHELL TRANSITION-METALS, *Physical Review B*, 1993, **48**, 13115-13118.
5. J. P. Perdew, K. Burke and M. Ernzerhof, Comment on "Generalized gradient approximation made simple" - Reply, *Physical Review Letters*, 1998, **80**, 891-891.
6. J. P. Perdew, K. Burke and M. Ernzerhof, Generalized gradient approximation made simple (vol 77, pg 3865, 1996), *Physical Review Letters*, 1997, **78**, 1396-1396.
7. M. Ropo, K. Kokko and L. Vitos, Assessing the Perdew-Burke-Ernzerhof exchange-correlation density functional revised for metallic bulk and surface systems, *Physical Review B*, 2008, **77**.
8. G. Y. Guo and H. H. Wang, Calculated elastic constants and electronic and magnetic properties of bcc, fcc, and hcp Cr crystals and thin films, *Physical Review B*, 2000, **62**, 5136-5143.
9. R. Soulairol, C. C. Fu and C. Barreteau, Structure and magnetism of bulk Fe and Cr: from plane waves to LCAO methods, *Journal of Physics-Condensed Matter*, 2010, **22**.
10. R. Hafner, D. Spisák, R. Lorenz and J. Hafner, Magnetic ground state of Cr in density-functional theory -: art. no. 184432, *Physical Review B*, 2002, **65**.
11. A. S. Belozerov, A. A. Katanin and V. I. Anisimov, Itinerant magnetism of chromium under pressure: a DFT plus DMFT study, *Journal of Physics-Condensed Matter*, 2021, **33**.
12. B. G. Janesko, Replacing hybrid density functional theory: motivation and recent advances, *Chemical Society Reviews*, 2021, **50**, 8470-8495.
13. P. W. Anderson, Localized Magnetic States in Metals, *Phys. Rev.*, 1961, **124**.
14. J. Hubbard, Electron Correlations in Narrow Energy Bands, *Proceedings of the Royal Society of London. Series A, Mathematical and Physical*, 1963, **276**, 238-257.
15. R. Shinde, S. Yamijala and B. M. Wong, Improved band gaps and structural properties from Wannier-Fermi-Lowdin self-interaction corrections for periodic systems, *Journal of Physics-Condensed Matter*, 2021, **33**.
16. G. Kresse and D. Joubert, From ultrasoft pseudopotentials to the projector augmented-wave method, *Physical Review B*, 1999, **59**, 1758-1775.
17. P. E. Blochl, PROJECTOR AUGMENTED-WAVE METHOD, *Physical Review B*, 1994, **50**, 17953-17979.
18. P. Pulay, CONVERGENCE ACCELERATION OF ITERATIVE SEQUENCES - THE CASE OF SCF ITERATION, *Chemical Physics Letters*, 1980, **73**, 393-398.
19. A. J. Pindor, J. Staunton, G. M. Stocks and H. Winter, DISORDERED LOCAL MOMENT STATE OF MAGNETIC TRANSITION-METALS - A SELF-CONSISTENT KKR CPA CALCULATION, *Journal of Physics F-Metal Physics*, 1983, **13**, 979-989.
20. W. M. T. G. M. Stocks, and B. L. Gyorffy, Complete Solution of the Korringa-Kohn-Rostoker Coherent-Potential-Approximation Equations: Cu-Ni Alloys, *Physical Review Letters*, 1978, **41**.
21. D. W. Taylor, VIBRATIONAL PROPERTIES OF IMPERFECT CRYSTALS WITH LARGE DEFECT CONCENTRATIONS, *Physical Review*, 1967, **156**, 1017-&.
22. P. Soven, COHERENT-POTENTIAL MODEL OF SUBSTITUTIONAL DISORDERED ALLOYS, *Physical Review*, 1967, **156**, 809-&.

23. I. N. S. Matsuo, K. Kimoto and S. Noguchi, *Journal of the Physical Society of Japan* 1978, **44**, 1387-1388.
24. E. C. Stoner., *Proceedings of the Royal Society of London. . Series A. Mathematical and Physical Sciences*, 1938, **165**, 372-414.
25. M. S. S. Brooks, Conduction electrons in magnetic metals. , *Matematisk-Fysiske Meddelelser*, 1997, **45**, 291-314.
26. I. Materials Design, MedeA.*Journal*, 2021.
27. J. L. Hénin, T.; Shirts, M. R.; Valsson, O.; Delemotte, L. , Enhanced Sampling Methods for Molecular Dynamics Simulations [Article v1.0], *Living Journal of Computational Molecular Science* 2022, **4**.
28. A. Togo and I. Tanaka, First principles phonon calculations in materials science, *Scripta Materialia*, 2015, **108**, 1-5.